3D Cell Cultures Amplify Diffusion Signals

Hamidreza Arjmandi[1], Kajsa P Kanebratt[2], Liisa Vilén[2], Peter Gennemark[2,3], and Adam Noel[1,*]

[1]School of Engineering, University of Warwick, Coventry, UK.
[2]Drug Metabolism and Pharmacokinetics, Research and Early Development, Cardiovascular, Renal and Metabolism (CVRM), AstraZeneca, Gothenburg, Sweden.
[3]Department of Biomedical Engineering, Linköping University, Sweden.
[*]adam.noel@warwick.ac.uk

ABSTRACT

Biophysical models can predict the behavior of cell cultures including 3D cell cultures (3DCCs), thereby reducing the need for costly and time-consuming experiments. Specifically, mass transfer models enable studying the transport of nutrients, oxygen, signaling molecules, and drugs in 3DCC which requires defining boundary conditions (BC) between the 3DCC and surrounding medium. However, accurately modeling the BC that relates the inner and outer boundary concentrations at the border between the 3DCC and the medium, remains a challenge that this paper addresses using both theoretical and experimental methods. The provided biophysical analysis indicates that the concentration of molecules at the inner boundary is higher than that at the outer boundary, revealing an amplification factor, which is confirmed by a particle-based simulator (PBS). Due to the amplification factor, the PBS confirms that when a 3DCC with a low concentration of target molecules is introduced to a culture medium with a higher concentration, the molecule concentration in the medium rapidly decreases. Liver spheroids are used as the 3DCC and glucose as the target molecule in the experiments. The PBS is leveraged to design these experiments, and results agree with our proposed theory and derived properties, particularly when having a higher medium volume.

Introduction

The term *3D cell culture (3DCC)* refers to any type of *in vitro* model in which cells are grown in three dimensions, as opposed to the traditional 2D monolayer culture. Organoid, spheroid, and tumouroid are all examples of 3DCC models, each with unique characteristics and applications. 3DCCs have received great attention and popularity in recent years due to their ability to better mimic the complex microenvironments and cell-cell interactions of *in vivo* tissues, in comparison to traditional 2D cell cultures. 3DCC can be composed of several different cell types, e.g., hepaotycyes and stellate cells to form liver spheroids. They can be used to model organ development and disease and have a wide range of applications in basic biological research, drug discovery, and regenerative medicine[5]. Organ-on-chips (OoCs) as bioengineered microdevices use the 3D nature and arrangement of 3DCCs to recapitulate key functional properties of organs and tissues[6].

Biophysical models are important mathematical and computational tools to describe physical and chemical properties of biological processes and systems including 3DCCs. They integrate biological data with mathematical equations or algorithms to simulate the behavior of the biological system[1–3]. These models are beneficial in 3DCC studies in several ways. Biophysical models can predict the behavior of 3DCCs under various conditions. Thus, they can be used to optimize the 3DCC conditions. Biophysical models can reduce the need for expensive and time-consuming experimental assays by predicting the outcomes under different experimental conditions. Also, we can use these models to integrate data from multiple scales[4] ranging from the molecular and cellular level to the tissue level to provide a comprehensive understanding of the behavior of 3DCCs. Furthermore, biophysical models may reveal new phenomena that may not be observable through experiments alone.

Mass transfer models are a crucial category of biophysical models that can enable researchers to study the transport of essential molecules, including nutrients, oxygen, signaling molecules, and drugs in 3DCCs. Specifically, the transfer of diffusible nutrients, like oxygen, plays a vital role in regulating fundamental cellular processes such as cell migration, death, and progression through the cell cycle[7,8]. 3DCCs rely on a culture medium that fills the void spaces and creates a continuous fluidic environment where molecules are transferred through two transport mechanisms, diffusion and flow, which contribute to the mass transfer model. When there is slow flow, or in avascular 3DCCs where there is no vascular system to deliver nutrients and oxygen, diffusion dominates the mass transfer model. Diffusion of molecules in an environment is described by Fick's laws of diffusion which are partial differential equations that describe the change in concentration of diffusing molecules with respect to time and space[9].

The diffusion of molecules within the medium outside and inside the 3DCC is modeled differently to account for the

varying physical and chemical properties of the porous culture. The 3DCC can be modeled as a porous medium with an equivalent diffusion coefficient that scales down the diffusion coefficient in the free culture medium. To model diffusion of molecules within the medium inside and outside the 3DCC, we can consider two diffusion environments with different diffusion coefficients. The concentration of diffusing molecules are characterized through two partial differential equations. These two equations are connected by defining two boundary conditions (BCs) at the 3DCC border that relates the concentration of molecules at inner and outer boundaries. The first BC is the flow continuity condition, which is applied at the border to ensure equal mass flux across the boundary. The second BC is characterized by the concentration ratio at the inner and outer border of the 3DCC[9]. This BC, referred to as the *amplification BC* throughout the rest of this paper, accounts for the influence of the 3DCC on the diffusive transport of molecules and has a significant impact on the accuracy of the diffusion model.

Despite its importance, the amplification BC has not been comprehensively characterized in the literature, and different types of models have been proposed by various authors. Some works define the amplification BC as a unitary ratio, implying that the concentration is the same inside and outside the 3DCC border[10–13]. Astrauskas et al. (2019) presented a reaction-diffusion equation model for analysis of dye penetration into cellular spheroids in which the unitary ratio is employed to model the boundary condition[10]. Leedale et al. (2020) developed a diffusion model of drug transport and metabolism that is developed in a multiscale spheroid framework, accounting for microscale processes where the concentration at the boundary is simply assumed to be equal to the outside concentration[11]. Bull et al. (2021) developed a hybrid, off-lattice agent-based model for oxygen-limited spheroid growth[12]. The concentration at the spheroid boundary is assumed to be maintained at the constant oxygen concentration in the culture medium, i.e., the unitary ratio is assumed. As part of his thesis, Rousset studies the molecule diffusion into and consumption by a spheroid where the unitary ratio is used to model the boundary condition[13].

In other works, a porosity ratio is assumed for BC, where the concentration at the inside boundary is expressed as the concentration outside the boundary multiplied by the porosity coefficient. Graff et al. (2003) develop a mathematical model to provide an improved understanding of the quantitative interplay among the rate processes of diffusion, binding, degradation, and plasma clearance in antibody penetration of tumour spheroids[14]. The authors consider the concentration at the spheroid boundary to be equal to the concentration outside multiplied by the spheroid porosity. In other words, they assume that the molecule concentration at the intercellular space boundary (i.e., void space at the spheroid's border) is equal to the concentration outside the spheroid. A similar boundary condition has been considered by Goodman et al. (2008), where the authors develop a mathematical model of nanoparticle penetration into multicellular spheroids that accounts for radially-dependent changes in tumour architecture[15].

Furthermore, some authors have modeled the diffusion process only inside the 3DCC, considering a constant concentration at the inner boundary, but not relating it to the concentration at the outer boundary[16,17]. Grimes et al. (2014) employ the oxygen diffusion model in three-dimensional tumour spheroids to present a method for estimating rates of oxygen consumption from spheroids[16]. The concentration at the boundary of the tumour is assumed constant and unrelated to the concentration in the surrounding media. In other words, a model with one diffusion environment is assumed where the concentration at the inner border is fixed. Klowss et al. (2022) develop a stochastic model that provides quantitative information about nutrient availability within the spheroid[17]. Similar to Grimes et al. (2014)[16], Klowss et al. (2022) only model the diffusion inside the spheroid given that the nutrient concentration at the boundary is constant equal to some maximum far-field concentration.

These diverse approaches demonstrate the ongoing challenge to accurately model the mass transport process in 3DCCs and motivates us to more accurately derive and characterize the amplification BC between 3D cell cultures and the surrounding media using theoretical and experimental methods. We use an equivalent diffusion model to describe the porous structure of 3DCC and determine the corresponding diffusion coefficient and concentration. To quantify the amplification BC, we analytically demonstrate that the concentration of molecules at the inner boundary is amplified relative to the concentration at the outer boundary by a factor that is greater than or equal to one, which we refer to as the *amplification factor*.

To provide an intuitive explanation for the boundary amplification factor, let us consider a 3DCC culture inside a microfluidic chip compartment or well that is exposed to a medium containing a known concentration of molecules. Due to the concentration gradient, molecules begin to enter the cell culture. However, the smaller diffusion coefficient within the cell culture matrix causes molecules that are freely diffusing in the well to become (relatively) trapped and absorbed within the matrix. As a result, we expect that molecules accumulate at the inner boundary of the 3DCC leading a higher concentration than at the outer boundary.

We have provided a particle-based simulator (PBS) that confirms the analytical result. The PBS reveals that a non-unitary amplification factor could lead to a noticeable impact on the molecule concentration in the medium when we add low-porous cell cultures to the medium. When a 3DCC containing a lower concentration of target molecules is placed in a medium with a higher concentration of these molecules, our PBS reveals a rapid decrease in the concentration of the molecules in the culture medium. This rapid behaviour as a result of the amplification factor in the amplification BC can explain the initial offset observations reported by Casas et al. (2022)[18] and similar 3DCC experiments. We leverage our proposed PBS to design additional experiments that provides a mechanistic explanation to the initial offset due to the amplification factor. Furthermore,

this experimental method can be used to characterize the amplification factor.

For our case study, we used liver spheroids as our 3DCC and glucose as our target molecule. Prior to introducing the liver spheroids to a medium with a high glucose concentration of 11 mM, **they were kept in two pre-culture media of volume 100 and 75 μL with a glucose concentration of 2.8 mM. Our experimental findings show a reduction in glucose concentration within the medium ($p = 0.008$ for 100 μL medium and $p = 0.06$ for 75 μL).** Additionally, our PBS results closely align with the experimental results, particularly when having higher medium volume.

The remainder of this paper is organized as follows. We present the theoretical modeling including the mathematical proof. Then, we introduce the experimental methods employed, beginning with our approach to revealing the rapid drop in medium concentration, followed by the proposed PBS to confirm our theoretical results and the designed experiment. Finally, the results and subsequent discussions are presented.

Theoretical Methods

Modeling of Diffusion BCs at the border of 3DCC

A 3DCC with volume V_s formed by N_c cells including $N_c^1, \cdots, N_c^Q$ of Q different types is considered. The culture's interior space is comprised of the cells and the void space between the cells (i.e., extracellular environment). Given that the volume of cell type i is V_c^i, the volumes of the cell matrix and the void space inside the 3DCC are given by $\sum_{i=1}^{Q} V_c^i N_c^i$ and $V_s - \sum_{i=1}^{Q} V_c^i N_c^i$, respectively.

We model the 3DCC structure as a porous medium with volume V_s whose porosity, ε, is defined as the ratio of the void space to the whole 3DCC volume, i.e.,

$$\varepsilon = 1 - \frac{\sum_{i=1}^{Q} V_c^i N_c^i}{V_s}. \tag{1}$$

We assume that the cell culture is in a fluid medium that surrounds it and fills its void space. The diffusive signaling molecules of type A in the medium can diffuse into the void space of the cell culture. In order to analyze the diffusion effect exclusively, we assume that there is no chemical reaction or binding occurring between the cells and target molecules within the cell culture structure. This assumption reasonably holds over a sufficiently short timescale when the culture is first exposed to the medium and the diffusion effect dominates. It is especially applicable when the rate of molecule binding and consumption is much slower than diffusion, such as in the case of glucose absorption by liver cells.

Ideally, the porous culture structure acts as a net, enabling molecules outside the cell culture to pass through its borders with a probability that depends on the surface porosity of the culture. This surface porosity can be estimated based on the geometrical projection of volume porosity (ε) in 3D into 2D using $\varepsilon_s = \varepsilon^{\frac{2}{3}}$. Inside the 3DCC, the molecules diffuse via the curved paths of the void space among the cells, which leads to a shorter net molecule displacement within a given time interval. Thus, macroscopic diffusion within the cell culture effectively differs from the diffusion within the free fluid outside it. Since the molecules traverse a shorter net path within the cell culture, the effective diffusion coefficient is smaller than the diffusion coefficient in the free fluid medium and molecules are more likely to be observed and sensed by the culture's cells (see Fig. 1). Given the diffusion coefficient D for molecules A in the free fluid, the effective diffusion coefficient within the cell culture is given by[21]

$$D_{\text{eff}} = \frac{\varepsilon}{\tau} D, \tag{2}$$

where τ is the tortuosity, a measure of the transport properties of the porous medium, and is modeled as a function of cell culture porosity as $\tau = \frac{1}{\sqrt{\varepsilon}}$[20].

These two diffusion environments inside and outside the 3DCC are connected by defining two boundary conditions (BCs) at the border of 3DCC. The first BC is the following flow continuity condition, which is applied at the border to ensure equal mass flux across the boundary:

$$D_{\text{eff}} \nabla c_s(\bar{r}, t) \cdot \hat{n} = D \nabla c_o(\bar{r}, t) \cdot \hat{n}, \quad \bar{r} \in \partial\Omega, \tag{3}$$

where $\partial\Omega$ denotes the boundary region of the cell culture, $\hat{n}$ is the normal vector at the border point $\bar{r}$, c_o is the concentration of molecules outside the cell culture, and c_s is the concentration of molecules inside the equivalent diffusion model of the cell culture, i.e., a free diffusion environment of volume V_s with diffusion coefficient D_{eff}. Thus, the concentration inside the void space within the cell culture is given by c_s/ε. For the two diffusion environments, the second BC is characterized by the concentration ratio at the inside and outside 3DCC border as[9]

$$c_s(\bar{r}, t) = k c_o(\bar{r}, t), \quad \bar{r} \in \partial\Omega \tag{4}$$

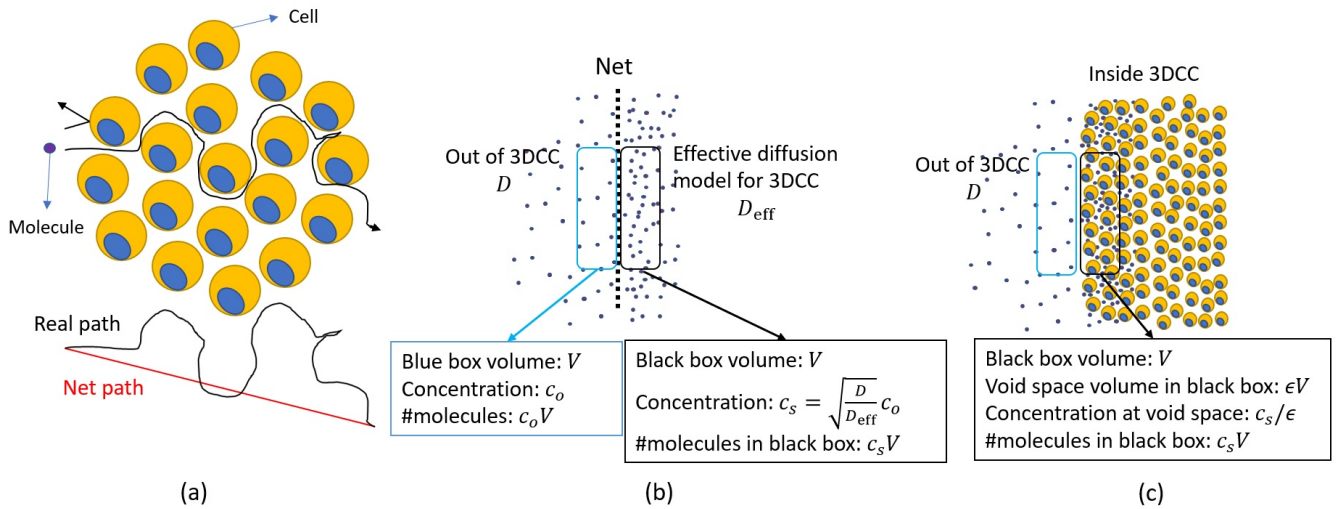

Figure 1. (a) Curved path of molecules within the spheroid leads to an effective diffusion coefficient smaller than the diffusion coefficient of the free medium, i.e., $D_{\text{diff}} < D$. (b) Boundary between media outside of 3DCC and the effective diffusion model for 3DCC which is a free medium diffusion environment with D_{diff}. The net (dashed line) at the boundary models the surface porosity and corresponding molecule reflection. The concentration and number of molecules at both sides are presented given a small volume very close to the boundary. (c) Boundary between media outside and inside 3DCC that includes both the cells and void space.

where k has not been derived and is suggested to be determined experimentally[9]. This is a common BC model used for the border of 3DCC with surrounding media. Despite its importance, this second BC for a 3DCC inside media has not been comprehensively or consistently characterized in the literature. However, the amplification factor should be derived as a function of porosity of the medium.

We refer to the BC (4) and k as the *amplification BC* and *amplification factor*, respectively. The amplification BC accounts for the influence of the 3DCC on the diffusive transport of molecules and has a significant impact on the accuracy of the diffusion model. We previously used a particle-based simulator for a system with a spheroid inside an unbounded environment as two ideal diffusion environments with diffusion coefficients D and D_{eff} and, without any net barrier, the simulation results suggested $k = \sqrt{\frac{D}{D_{\text{eff}}}}$ [22]. Here, we theoretically prove that $k = \sqrt{\frac{D}{D_{\text{eff}}}}$ generally characterizes the amplification BC for a 3DCC inside a medium modeled as two diffusion environments separated by a net border with porosity of ε_s. Since the boundary is assumed to be ideal, a particle that passes the border will follow its arrival direction and not change direction. As a result, we can assume a one-dimensional diffusion environment for the proof, without any loss of generality.

Proposition 1: For two ideal diffusion environments with diffusion coefficients D and D_{eff} separated by a net surface with porosity ε_s and concentration functions $c_o(x), x \in [-\infty, 0]$ and $c_s(x), x \in [0, \infty]$, the amplification factor is equal to

$$k = \sqrt{\frac{D}{D_{\text{eff}}}}. \tag{5}$$

Proof: During a very short time interval Δt, the molecules within the left side region $x \in [-3\sigma_o, 0]$ (where $\sigma_o = \sqrt{2D\Delta t}$) have a realistic chance to pass across the boundary to the right. Within a small region with length dx at any point $x \in [-3\sigma_o, 0]$, we have $c_o(x)\mathrm{d}x$ molecules that may pass the boundary with the probability $\int_{-x}^{+\infty} \frac{1}{\sqrt{2\pi}\sigma_o} \exp\left(-\frac{u^2}{2\sigma_o^2}\right) \mathrm{d}u$. Therefore, the total number of molecules crossing the boundary from the left side over Δt seconds is $\varepsilon_s \int_{-3\sigma_o}^{0} \int_{-x}^{+\infty} \frac{c_o}{\sqrt{2\pi}\sigma_o} \exp\left(-\frac{u^2}{2\sigma_o^2}\right) \mathrm{d}u\mathrm{d}x$. This can be rewritten as $\varepsilon_s \int_0^{3\sigma_o} \int_{|x|}^{+\infty} \frac{c_o}{\sqrt{2\pi}\sigma_o} \exp(-\frac{u^2}{2\sigma_o^2}) \mathrm{d}u\mathrm{d}x$.

Similarly, we can derive an expression for the number of molecules that move from the right to the left side of the boundary as $\varepsilon_s \int_0^{3\sigma_s} \int_{|x|}^{+\infty} \frac{c_s}{\sqrt{2\pi}\sigma_s} \exp(-\frac{u^2}{2\sigma_s^2}) \mathrm{d}u\mathrm{d}x$. On the other side, the molecule flux at the boundary is given by (3) in one dimension, i.e., $D\frac{dc_o}{dx}$. During a very short time interval Δt, this flux leads to the passage of $D\frac{\mathrm{d}c_o}{\mathrm{d}x}\Delta t$ molecules across the boundary. Thus,

we can write

$$\varepsilon_s \int_0^{3\sigma_o} \int_{|x|}^{+\infty} \frac{c_o}{\sqrt{2\pi}\sigma_o} \exp\left(-\frac{u^2}{2\sigma_o^2}\right) \mathrm{d}u\mathrm{d}x - \varepsilon_s \int_0^{3\sigma_s} \int_{|x|}^{+\infty} \frac{c_s}{\sqrt{2\pi}\sigma_s} \exp\left(-\frac{u^2}{2\sigma_s^2}\right) \mathrm{d}u\mathrm{d}x = D\frac{\mathrm{d}c_o}{\mathrm{d}x}\Delta t. \tag{6}$$

By making the substitution $u = \frac{\sigma_s}{\sigma_o}u'$ in the second term on left side and defining $F(x) = \int_{|x|}^{+\infty} \frac{1}{\sqrt{2\pi}\sigma_o} \exp\left(-\frac{u^2}{2\sigma_o^2}\right) \mathrm{d}u$, we obtain

$$\varepsilon_s \int_0^{3\sigma_o} c_o(x)F(x)\mathrm{d}x - \varepsilon_s \int_0^{3\sigma_s} c_s(x)F\left(\frac{\sigma_o}{\sigma_s}x\right)\mathrm{d}x = D\frac{\mathrm{d}c_o}{\mathrm{d}x}\Delta t. \tag{7}$$

By making the substitution $x' = \frac{\sigma_o}{\sigma_s}x$, we get

$$\int_0^{3\sigma_o} c_o(x)F(x)\mathrm{d}x - \int_0^{3\sigma_o} c_s\left(\frac{\sigma_s}{\sigma_o}x'\right)\frac{\sigma_s}{\sigma_o}F(x')\mathrm{d}x' = \frac{D}{\varepsilon_s}\frac{\mathrm{d}c_o}{\mathrm{d}x}\Delta t. \tag{8}$$

For a very short Δt, as σ_0 approaches zero, we can approximate $c_o(x)$ and $c_s(x)$ as constant values equal to $c_o(0^-)$ and $c_s(0^+)$ respectively within the integral bounds of $[0, 3\sigma_0]$. Therefore, (8) leads to

$$\left(c_o(0^-) - c_s(0^+)\frac{\sigma_s}{\sigma_o}\right)\int_0^{3\sigma_o} F(x)\mathrm{d}x = \frac{D}{\varepsilon_s}\frac{\mathrm{d}c_o}{\mathrm{d}x}\Delta t. \tag{9}$$

Note that a change of variable simplifies $F(x) = \int_{|x|/\sigma_o}^{+\infty} \frac{1}{\sqrt{2\pi}} \exp(-\frac{u^2}{2})du = Q(|x|/\sigma_o)$ where $Q(\cdot)$ is the Q-function. Furthermore, by one additional variable change, we obtain

$$\int_0^{3\sigma_o} F(x)dx = \int_0^{3\sigma_o} Q(|x|/\sigma_o)dx = \sigma_o \int_0^3 Q(x)\mathrm{d}x \simeq 0.4\sigma_o.$$

Therefore, (9) is written as

$$(c_o(0^-) - c_s(0^+)\frac{\sigma_s}{\sigma_o})0.4\sigma_o = \frac{D}{\varepsilon_s}\frac{\mathrm{d}c_o}{\mathrm{d}x}\Delta t. \tag{10}$$

Considering $D\Delta t = \sigma_o^2/2$, we obtain

$$(c_o(0^-) - c_s(0^+)\frac{\sigma_s}{\sigma_o})0.8\varepsilon_s = \frac{\mathrm{d}c_o}{\mathrm{d}x} \times \sqrt{2D\Delta t}. \tag{11}$$

Obviously, as $\Delta t \to 0$, the right side goes to zero, which implies that $\sigma_o c_o(0^-) = \sigma_s c_s(0^+)$ or equivalently $k = \frac{\sigma_o}{\sigma_s} = \sqrt{\frac{D}{D_{\text{eff}}}}$. The proof is complete.

Thus, for $k \neq 1$, a concentration discontinuity (i.e., jump) occurs at the boundary. Therefore, the concentration is amplified when passing across the cell culture by factor k. The proof is complete.

We note that kc_o is the inner boundary concentration of the equivalent free diffusion environment with diffusion coefficient D_{eff}. Therefore, the concentration at the boundary extracellular matrix of the cell culture would be $\frac{kc_o}{\varepsilon}$.

Experimental Methods

In this section, we discover and analyze an emergent property of 3DCCs caused by the amplification factor acting at the culture boundary. This property can influence the outcomes and interpretations of experiments involving 3DCCs. To measure and characterize the amplification factor, we utilize this property to design an *in vitro* experiment in which the liver spheroids are exposed to a fluid medium with glucose molecules. We use a particle-based simulator that accurately emulates the experimental activity and enables us to gain further insights into the relevant parameters required to carry out the experiment.

Rapid concentration reduction in culture medium

To provide an intuitive explanation for the boundary amplification factor, let us consider a 3DCC culture inside a microfluidic chip compartment or experimental well that is exposed to a medium containing a known concentration of molecules. Due to the concentration gradient, molecules begin to enter the cell culture. However, the smaller diffusion coefficient within the cell culture matrix causes molecules that are freely diffusing in the well to become (relatively) trapped and absorbed within the matrix. In other words, due to the small effective diffusion coefficient inside the cell culture, it takes a longer time for molecules to exit.

As a result, we expect that molecules accumulate within the cell culture, thus reducing the concentration of the molecules in the medium, provided that there are no reactions between cells and molecules that occur faster than the transient diffusion behavior. This phenomenon is a consequence of the amplification factor that comes from the smaller effective diffusion coefficient inside the cell culture. Obviously, the concentration reduction would be more significant for larger cell culture volumes and higher amplification factors. To provide a preliminary estimate of the concentration change, let us make some simplifying assumptions and perform some quick insightful calculations.

Let us consider a well that is filled with a medium of volume V_m and a molecule concentration of C_m. Next, we introduce N_c 3DCCs, such as spheroids, to the medium. Prior to this, the cell cultures were maintained in a pre-culture medium with a concentration $C_p < C_m$. Initially, the molecule concentration in the spheroids is expected to be $C_s < kC_p$, assuming no reaction or consumption of the molecules, with a homogeneous distribution of molecules within the spheroids, and keeping the pre-culture medium concentration at a constant C_p.

We can assume that each spheroid contains C_sV_s molecules at the time of being added to the well. After a brief period of time, numerous molecules are expected to have diffused into the spheroids due to the concentration gradient. We can further assume that molecule reactions with the cells is significantly slower than the diffusion rate within the spheroids. As a result, no molecule is lost due to reaction during the transient period when there is net diffusion of molecules into the spheroid.

Under these conditions, the molecule concentration within the spheroid will increase and eventually reach a local time equilibrium C_s'. At the same time, the molecule concentration in the medium decreases to a constant average level denoted by C_m'.

By local time equilibrium, we mean that the concentration throughout the whole spheroid(s) will be uniform for that short time. Given the boundary condition in (4), the concentration inside the spheroid will be $C_s' = kC_m'$. To obtain C_s' and C_m', we consider the molecule conservation in this closed system. The total number of molecules at time $t = 0$ was $C_mV_m + N_sC_sV_s$ which is equal to the number of molecules shortly thereafter at the local time equilibrium. Therefore, we have

$$C_m'V_m + N_sC_s'V_s = C_mV_m + N_sC_sV_s. \tag{12}$$

By applying $C_s' = kC_m'$ and the bound $C_s < kC_p$, we obtain

$$C_m' < \frac{C_mV_m + N_skC_pV_s}{V_m + kN_sV_s}. \tag{13}$$

Equivalently, the concentration reduction in the medium is obtained as

$$C_m - C_m' \geq \frac{(C_m - C_p)kN_sV_s}{V_m + kN_sV_s}. \tag{14}$$

From 14, a higher k value could further reduce the medium concentration inside the well while increasing the concentration inside the cell culture. However, this analysis is valid at equilibrium, and the exact time-point when this equilibrium occurs is unknown to us. On the other hand, if we wait too long to measure, then the biochemical reactions in the cell pathways may significantly affect the molecule concentration inside the spheroids. In particular, for our experiments, the liver cells take up glucose molecules. To better clarify these points, we use a particle-based simulator that is able to track transient molecule concentration and we use liver cells taking up glucose molecules in our experiments, which is known to be much slower (i.e., hours) than the diffusion process[23].

Particle-based simulator

We use liver spheroids created by differentiated HepaRG cells and human hepatic stellate cells following the method described by Bauer et al. (2017)[23] for our simulations and experiments. Figure 2 displays images of six spheroids that were formed using this method, shown at two different scales. Each image displays the maximum projected area of a spheroid in 2D. To determine the spheroid's area within the image, the software tool ImageJ[24] was utilized, and the radius of a circle with equivalent area is used as the spheroid's radius. The average spheroid radius across these 6 samples was found to be $R_s = 226$ μm. The

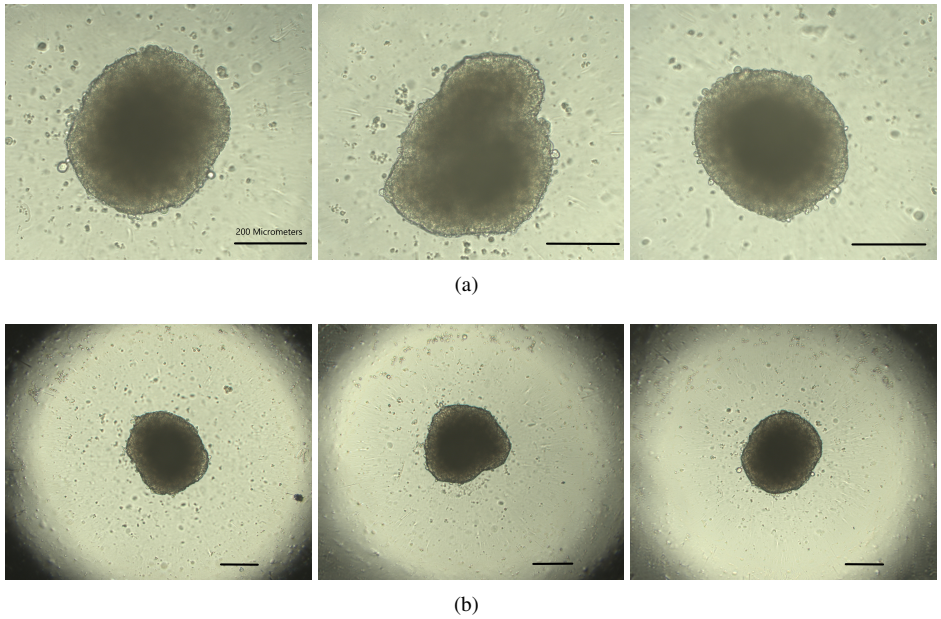

Figure 2. (a) Microscopic images of three liver spheroids at 10X magnification (scale bar is 200 μm). (b) Microscopic images of three spheroids at 4X magnification (scale bar is 200 μm).

total number of cells in each spheroid is assumed to be $N_c = 25000$ including 24000 HepaRG cells and 1000 human hepatic stellate cells, as reported by Bauer et al. (2017)[23], with cell volumes of 1.7×10^{-15} and 1.1×10^{-15} m^3, respectively. Using $N_c = 25000$, we obtain $\varepsilon = 0.1$ and correspondingly $k = 4.49$.

We considered a flat-bottomed well with a radius of $R_w = 3.2$ mm and a height of 6.2 mm for our *in vitro* experiments. We chose to use medium volumes of $V_m = \{100, 75\}$ μL. To demonstrate the amplification factor and resulting concentration reduction in the culture medium, we chose a high glucose concentration of 11.2 mM (hyperglycemia)[23] in the well medium and a low glucose concentration of 2.8 mM in the pre-culture medium used to keep the spheroids alive. The large difference between these two concentrations helps to highlight the effect of the amplification factor.

To simulate the concentrations of 11.2 mM and 2.8 mM glucose in the culture and pre-culture media, respectively, with particle-based simulations, we would require a very large number of molecules and that is not computationally feasible. However, since the molecules move independently in the PBS, we do not need to use the exact number of molecules corresponding to these concentrations. Instead, we randomly placed $N_m = C_m V_m = 10^6$ molecules within the medium space and $N_s = C_s V_s = kC_p V_s$ molecules within each spheroid, which leads to the same ratio of 11.2:2.8 between the medium and pre-culture medium. We normalized the concentration values by the initial concentration inside the medium, which was set to 1, in order to demonstrate the results.

In the PBS, time is divided into time steps of $\Delta t = 0.1$ s. In each time step, the molecule locations are updated following random Brownian motion. The molecules move independently in the 3-dimensional space, either in the medium or within the spheroids where the displacement of a molecule in Δt s is modeled as a Gaussian random variables both with zero mean and variances $2D\Delta t$ and $2D_{\text{eff}}\Delta t$, respectively, along each dimension (Cartesian coordinates), where $D = 10^{-9}$ and $D_{\text{eff}} = 4.2 \times 10^{-11}$ m^2/s obtained from (2).

In reality, the movement of molecules outside the spheroid may be affected by the porous surface of the spheroid. Molecules may pass through the void spaces of the surface or reflect back if they hit other parts of the surface. For the simulation, the surface porosity of the spheroid is represented by the probability ε_s, which is the likelihood that a hitting molecule will enter the surface. For molecules inside the spheroid, we assume an equivalent diffusion environment with an effective diffusion coefficient D_{eff}.

We note that in this simplified environment model, the molecules can move freely inside the spheroid, and the porous structure effect is taken into account by using the effective diffusion coefficient. However, like the molecules outside, the molecules diffusing inside the equivalent environment may collide with the spheroid wall and exit with a probability of ε_s. We note that the opening sites over the boundary enables the passage of molecules in both directions, i.e., from the outside to the inside of the spheroid and vice versa. Consequently, we assume an equal probability of ε_s for movement in either direction.

Considering the mismatch between the diffusion coefficients, we need to update the displacement vector of a molecule that

crosses the spheroid boundary. For example, consider that a molecule in the medium outside a spheroid and its displacement vector during Δt s is $(\Delta x, \Delta y, \Delta z)$ with a length of d_T that would move the molecule into the spheroid. This vector has two parts: one part of length d_o outside the spheroid and one part of length d_i inside the spheroid. Then, the vector length for the inside part needs to be scaled by the factor $\sqrt{\frac{D}{D_{\text{eff}}}}$. As a result, the displacement vector is updated as follows

$$\frac{d_o + (\sqrt{\frac{D}{D_{\text{eff}}}} d_i)}{d_T} (\Delta x, \Delta y, \Delta z). \tag{15}$$

Similarly, if a molecule moves from inside to outside of the spheroid, then we need to update displacement vector outside according to

$$\frac{d_i + (\sqrt{\frac{D}{D_{\text{eff}}}} d_o)}{d_T} (\Delta x, \Delta y, \Delta z). \tag{16}$$

We also consider the cases where molecules diffusing within the well environment may hit the well walls or the top surface of medium. In all these cases, the molecules are reflected back inside the well.

Figure 3(a) presents the normalized glucose concentration (NGC) both inside and outside the spheroid for medium volumes of 75 and 100 μL. The arrows indicate the ratio of NGC inside the spheroid to NGC outside, which is found to be approximately $k = \sqrt{\frac{D}{D_{\text{eff}}}}$, as derived in (5). In Fig. 3(b), we show a higher resolution view of NGC in the medium for both volumes. The figure suggests that measuring the time-averaged NGC in the first 10 minutes provides a good estimate of the NGC reduction due to the spheroids. Fig. 3(c) shows that the predicted time-averaged GC for medium volumes of 75 and 100 μL over a period of 10 minutes is found to be 10.37 and 10.58, respectively, corresponding to a 5.7 and 3.8 percent GC reduction in the media, respectively. Therefore, in experiments we take samples at times 1, 5, and 10 minutes (min) after addition of spheroids to high-glucose medium to estimate the time-averaged NGC during the first 10 min, as chemical reactions may have a significant impact at longer timescales. We calculated the number of experiments required to achieve a power of 80 percent to distinguish these GC reductions from 11 mM, considering a variance of 0.15 for measurements and a significance level of 0.1. The required number of experiments is 3 and 4 for the two cases, respectively, to achieve a power of 80 percent. However, we opted to conduct 8 replicates for each case to achieve a higher level of confidence.

Liver Spheroid Formation and Glucose Assay

Formation of liver spheroids is based on the method published by Bauer et al. (2017)[23]. Differentiated HepaRGs (Lot HPR116239) were obtained from Biopredic International (Rennes, France). Primary human hepatic stellate cells (HHSteC), lot PFP, were purchased from BioIVT (Brussels, Belgium).

The differentiated HepaRGs were thawed and seeded confluently three days before spheroid formation. Standard HepaRG culture medium consisted of William's Medium E without glucose (PAN-Biotech, Aidenbach, Germany) supplemented with 10% foetal bovine serum (Gibco, ThermoFisher Scientific, Waltham, MA, USA), 11.1 mM glucose (Sigma–Aldrich, St. Louis, MO, USA), 5 μg/mL human insulin (Gibco), 2 mM L-glutamine (Corning), 50 μM hydrocortisone hemisuccinate (Sigma–Aldrich), 50 μg/mL gentamycin sulfate (Gibco) and 0.25 μg/mL Amphotericin B (Gibco). On the following day, the medium was renewed with HepaRG medium containing 2% dimethyl sulfoxide. The cells were maintained in this medium for two days until spheroid formation. HHSteC were expanded in Stellate Cell Medium, provided by ScienCell (Carlsbad, CA, USA). Cells were used in passage 3. Pre-culture was started two days before spheroid formation.

Human liver spheroids were formed combining differentiated HepaRG cells and HHSteC using 384-well spheroid microplates (Corning, Lowell, MA, USA) in HepaRG medium. Briefly, 50 μL containing 24,000 hepatocytes and 1,000 HHSteC was pipetted into each well of the spheroid plate. The plate was centrifuged for 1 min at 300 xg and incubated at 37 °C and 5% CO2. Two days after seeding, 20 μL medium was removed and 50 μL fresh medium was added to the spheroids and five days after seeding 50% medium was renewed.

Six days after seeding, 40 spheroids were pooled into a 24-well ultra low attachement plate (Corning). The spheroids were washed once with 500 μL HepaRG medium with 2.8 mM glucose and 1 nM insulin. After the wash, 800 μL of this medium was added and spheroids were incubated for 2h. Spheroids were then transferred to a 96-well flat bottom ultra low attachment plate (Corning) and medium was changed to 75 or 100 μL (8 replicates per volume) HepaRG medium with 11.1 mM glucose and 870 nM insulin. Medium samples were taken after 1, 5, and 10 min and HepaRG medium with 11 mM glucose and 870 nM insulin was sampled as 0 min control. For samples where starting volume was 100 μL, a medium sample was also taken after 4 h. For samples with starting volume of 75 μL, all medium was removed after 10 min sampling and 100 μL new medium was added. From these incubations medium was sampled after 19 h.

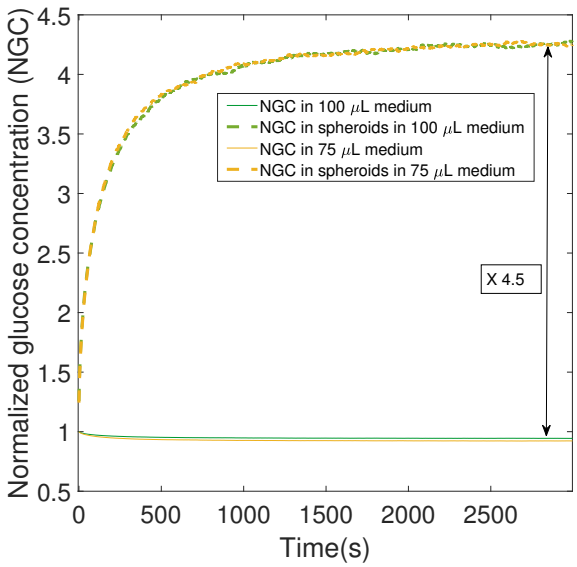

(a)

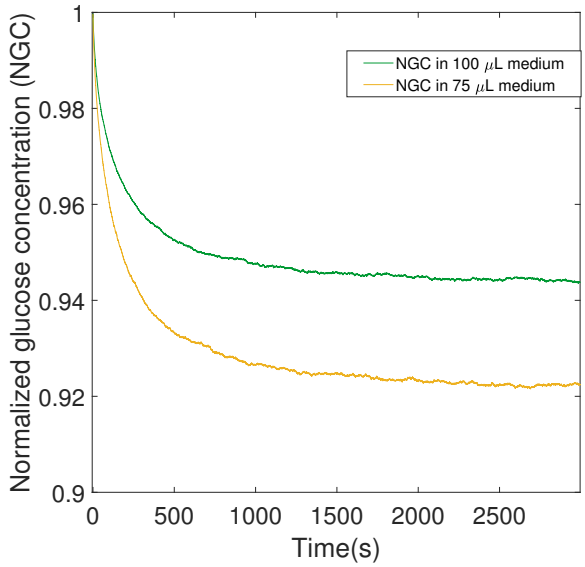

(b)

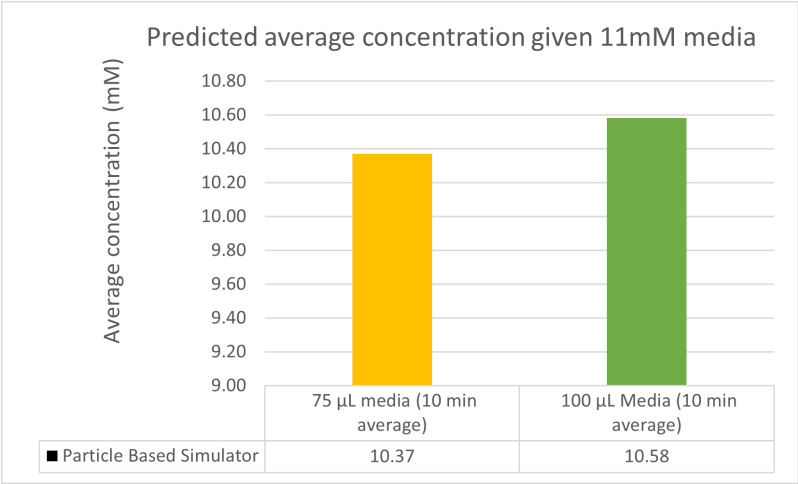

(c)

Figure 3. (a) Normalized glucose concentration (NGC) inside and outside the spheroid as a function of time for both medium volumes of 75 and 100 μL obtained by PBS. NGC inside the spheroids is the average over all 40 spheroids in the well. (b) A higher resolution view of NGCs in the medium for both volumes provided in Fig. 3(a). (c) The predicted time-averaged GC for medium volumes of 75 and 100 μL after a period of 10 minutes based on the results in Fig. 3(b).

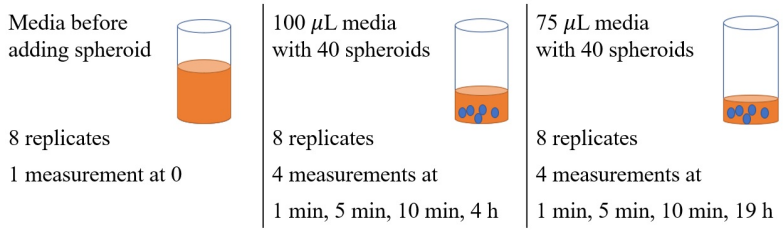

Figure 4. Schematic representation of *in vitro* experiment with summarized features.

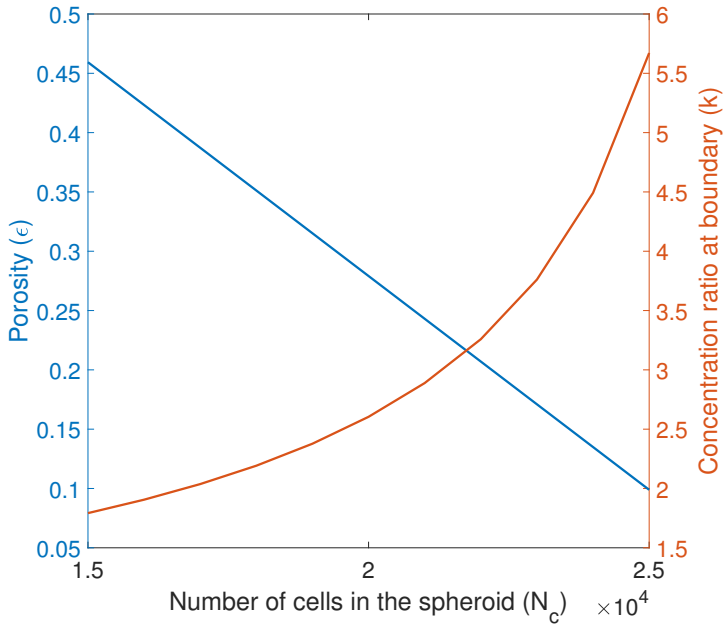

Figure 5. Porosity (ε) and concentration ratio at the boundary (k) versus the number of cells inside the spheroid (N_c).

After sampling, the medium was frozen and kept at -80 °C until analysis. Glucose concentrations in the samples were measured using Stanbio Glucose LiquiColor test. All samples were analysed undiluted according to manufacturer's instructions. In short, 5 μL sample or standard was added to a clear flat bottom 96-well plate (Nunc). The glucose reagent was pre-heated to 37 °C and the 95 μL reagent was added to start the reaction. The plate was centrifugated in short-spin to remove air bubbles and then incubated at 37 °C for 5 min. After incubation absorbance were directly measured at 520 nm on a Spectramax Plus reader and sample concentrations were calculated from standard curve.

Results

Fig. 5 demonstrates the porosity (ε) and amplification factor (k) as a function of the number of cells, $15000 < N_c < 25000$ in the spheroid given a fixed radius $R_s = 226\ \mu$m. The cell volume is assumed to be $V_c = 1.7 \times 10^{-15}$ m^3. As observed in Fig. 1, k increases exponentially with an increase in N_c. For $N_c = 25000$, which is the approximate number of cells in HepaRG spheroids reported[23], we have $\varepsilon = 0.1$ and correspondingly $k = 4.49$. This value of k suggests a large concentration discontinuity at the spheroid boundary.

Figs. 6(a) and 6(c) illustrate the outcomes of 8 replicates with incubation volumes of 100 μL and 75 μL. For each replicate, the glucose concentration was measured at 1, 5, and 10 min after addition of spheroids to the high-glucose medium. **Figs. 6(b) and 6(d) present the average of three initial samples at 1, 5, and 10 min (shown by green and orange bars, respectively) for each replicate and the statistical average (mean) of all replicates (shown by the purple bar). The obtained average can be interpreted as the 10-mean approximated average of glucose concentration**. The mean glucose concentration for the 100 and 75 μL incubations is observed to be 10.67 and 10.86 M, respectively.

Fig. 7(a) illustrates the mean glucose concentration in the spheroid-free medium, the mean time-averaged glucose

(a) (b)

(c) (d)

Figure 6. (a,c) Glucose concentration measured at 1, 5, and 10 minutes after introducing the spheroid to the medium for 8 replicates of for the 100 and 75 μL incubations, respectively. (b,d) The 10-minute time-averages of measured concentration at 1, 5, and 10 min for each replicate and the statistical average (mean) of the replicates (shown by the purple bar).

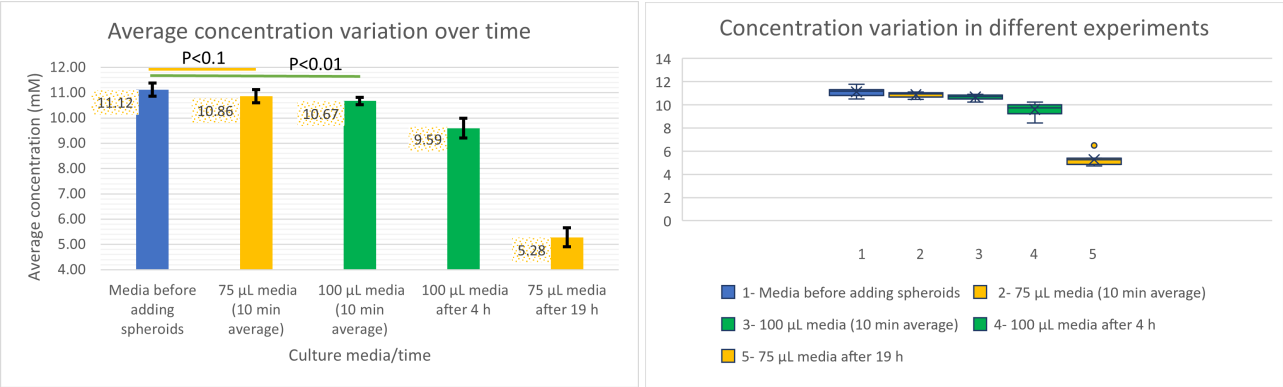

(a) (b)

Figure 7. (a) Mean GC in medium before adding spheroids, mean 10 min time-averaged GC for the 100 and 75 μL incubations, mean GC at 4 hours (for 100 μL), mean GC at 19 hours (for 75 μL) (b) Boxplot of the results.

concentration during the first 10 minutes approximated based on measurements at 1, 5, and 10 min for the 100 and 75 μL incubations, and the glucose concentration mean at 4 hours (for 100 μL) and 19 hours (for 75 μL). A box plot of these data is presented in Fig. 7(b), which confirms that there are no outliers based on the "median and quartiles" method, except for one that is negligible for the 19-hour samples.

The viability of the spheroids is evident from the reduction in glucose levels observed after 4 and 19 hours. Furthermore, the data shows a noticeable decrease in glucose concentration during the initial 10 minutes in both 75 and 100 μL incubations, which is more pronounced than the reduction observed after 4 hours due to glucose utilization by HepaRG cells. This finding supports the proposed theory of an amplification factor that leads to rapid glucose reduction over the timescale of initial transient diffusion. It also indicates that glucose absorption by HepaRG cells is a slow process and may not have a significant impact over this initial period. To test this hypothesis, we conducted two hypothesis tests.

The first hypothesis test compares the mean glucose concentration in the spheroid-free medium (μ_0) to the mean observed from the 100 μL experiment (μ_{100}). The null hypothesis is that the two means are equal ($\mu_0 = \mu_{100}$), while the alternative hypothesis is that the mean of the spheroid-free medium is greater than the mean of the 100 μL experiment ($\mu_0 > \mu_{100}$).

Similarly, the second hypothesis test compares the mean values for the 75 μL and spheroid-free experiments. The null hypothesis is that the mean glucose concentration in the spheroid-free medium is the same as the mean observed from the 75 μL incubation ($\mu_0 = \mu_{75}$), while the alternative hypothesis is that the mean of the spheroid-free medium is greater than the mean of the 75 μL incubation ($\mu_0 > \mu_{75}$).

The mean glucose concentrations observed in the medium before addition of spheroids, 100 μL, and 75 μL incubations are 11.12, 10.67, and 10.86, respectively. The corresponding variances of the data samples are 0.15, 0.05, and 0.049. Due to the differing variances in the data sets, we use a two-sample t-Test assuming unequal variances. It is worth noting that the different variances result from using the time-average of the experimental samples. We perform a one-tailed test due to the form of the alternative hypothesis.

The resulting p-values for the first and second tests are 0.008 and 0.06, respectively. These values indicate a strongly significant difference for the first hypothesis and a marginally significant difference for the second hypothesis. Based on these results, we can conclude that the spheroids lead to a statistically significant reduction in glucose concentration during the initial 10 minutes.

In addition to the hypothesis testing, we have compared our experimental results with the glucose concentration predicted by the PBS in Fig. 8. As observed, the PBS closely follows our experimental results for both experiments. We note that the presented PBS can only be used for comparison over a short timescale. Thus, there is no comparison made with PBS at 4h/19h.

Conclusion

To enable the development of reliable biophysical models for 3DCC, we utilized both theoretical and experimental methods to derive and characterize the amplification BC, which relates the inner and outer boundary concentrations at the border between 3DCC and its surrounding medium. Our biophysical theoretical analysis revealed an amplification factor that characterizes the amplification BC and that the factor is a function of the two diffusion coefficients of the cell culture and medium. We confirmed this analytical result using a proposed particle-based simulator (PBS), which also showed a rapid decrease in the molecule

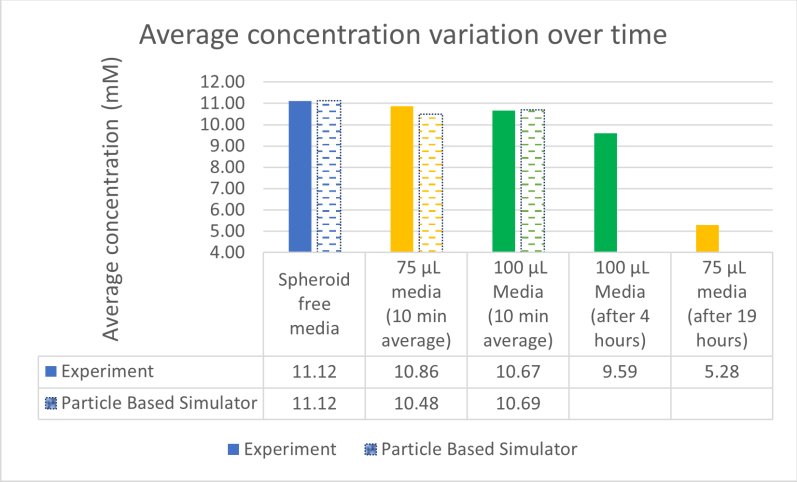

Figure 8. Experimental glucose concentration in the media compared with the predicted values obtained from the proposed PBS, assuming an initial concentration of 11.12 mM.

concentration in the culture medium as a result of the amplification factor. To evaluate our approach, we conducted experiments using a liver spheroid as the 3DCC and glucose as the target molecule. Our experiments demonstrated a significant reduction in glucose concentration within the medium, $p = 0.008$ for 100 μL medium and $p = 0.06$ for 75 μL, and the results closely aligned with the PBS simulations.

The amplification factor revealed through our theoretical and experimental methods has significant implications for biophysical models used in 3DCC experiments, including organ-on-a-chip models. Consideration of the amplification factor in such models would result in more accurate predictions of the behavior of 3DCCs, and consequently, aid in drug design and analysis of drug dosages within tissues. This factor may provide insight into the mechanism behind tumor development and morphogenises. In particular, the packed structure of cancer tumors enables them to receive and trap a higher concentration of nutrients and oxygen molecules based on the amplification factor. Thus, this study could contribute to the development of novel approaches to manage and treat cancerous tissues. Furthermore, our study offers a generic experimental approach to quantify the amplification factor for different 3DCCs and contributes to a better understanding of this phenomenon. This type of advanced *in vitro* modeling will likely play a major role in future drug discovery, providing a cost-effective human cell system with fewer ethical issues than animal models.

References

1. Bellocchi G, Rivington M, Donatelli M, Matthews K. Validation of biophysical models: issues and methodologies. *A review. Agronomy for Sustainable Development*, 30(1), 109-30, (2010).
2. Tracqui P. Biophysical models of tumour growth. *Reports on Progress in Physics*, 72(5), 056701, (2009).
3. Jelescu IO, Palombo M, Bagnato F, Schilling KG. Challenges for biophysical modeling of microstructure. *Journal of Neuroscience Methods*, 344, 108861, (2020).
4. McCulloch AD. Systems biophysics: multiscale biophysical modeling of organ systems. *Biophysical journal*, 110(5), 1023-7, (2016).
5. Rossi G, Manfrin A, Lutolf MP. Progress and potential in organoid research. *Nature Reviews Genetics*, 19(11), 671-87, (2018).
6. Low LA, Mummery C, Berridge BR, Austin CP, Tagle DA. Organs-on-chips: into the next decade. *Nature Reviews Drug Discovery*, 20(5), 345-61, (2021).
7. Ward JP, King JR. Mathematical modelling of avascular-tumour growth. *Mathematical Medicine and Biology: A Journal of the IMA*, 14(1), 39-69, (1997).
8. Haass NK, Beaumont KA, Hill DS, Anfosso A, Mrass P, Munoz MA, Kinjyo I, Weninger W. Real-time cell cycle imaging during melanoma growth, invasion, and drug response. Pigment cell & melanoma research, 27(5), 764-76, (2014).
9. Crank J. *The mathematics of diffusion*. (Oxford university press, 1979).

10. Astrauskas R, Ivanauskas F, Jarockytė G, Karabanovas V, Rotomskis R. Modeling the uptake of fluorescent molecules into 3D cellular spheroids. *Nonlinear analysis: modelling and control*, 24(5), 838-52, (2019).
11. Leedale JA, Kyffin JA, Harding AL, Colley HE, Murdoch C, Sharma P, Williams DP, Webb SD, Bearon RN. Multiscale modelling of drug transport and metabolism in liver spheroids. *Interface focus*, 10(2), 20190041, (2020).
12. Bull JA, Mech F, Quaiser T, Waters SL, Byrne HM. Mathematical modelling reveals cellular dynamics within tumour spheroids. *PLoS computational biology*, 16(8), e1007961, (2020).
13. Rousset N. Developing Modeling Approaches For Microfluidic Drop Networks. (Doctoral dissertation, ETH Zurich, 2022).
14. Graff CP, Wittrup KD. Theoretical analysis of antibody targeting of tumor spheroids: importance of dosage for penetration, and affinity for retention. *Cancer research*, 63(6), 1288-96, (2003).
15. Goodman TT, Chen J, Matveev K, Pun SH. Spatio-temporal modeling of nanoparticle delivery to multicellular tumor spheroids. *Biotechnology and bioengineering*, 101(2), 388-99, (2008).
16. Grimes DR, Kelly C, Bloch K, Partridge M. A method for estimating the oxygen consumption rate in multicellular tumour spheroids. *Journal of The Royal Society Interface*, 11(92), 20131124, (2014).
17. Klowss JJ, Browning AP, Murphy RJ, Carr EJ, Plank MJ, Gunasingh G, Haass NK, Simpson MJ. A stochastic mathematical model of 4D tumour spheroids with real-time fluorescent cell cycle labelling. *Journal of the Royal Society Interface*, 19(189), 20210903, (2022).
18. Casas B, Vilén L, Bauer S, Kanebratt KP, Wennberg Huldt C, Magnusson L, Marx U, Andersson TB, Gennemark P, Cedersund G. Integrated experimental-computational analysis of a HepaRG liver-islet microphysiological system for human-centric diabetes research. *PLOS Computational Biology*, 18(10), e1010587, (2022).
19. Daunys S, Janonienė A, Januškevičienė I, Paškevičiūtė M, Petrikaitė V. 3D tumor spheroid models for in vitro therapeutic screening of nanoparticles. *Bio-Nanomedicine for Cancer Therapy*, 243-70, (2021).
20. Sharifi F, Firoozabadi B, Firoozbakhsh K. Numerical investigations of hepatic spheroids metabolic reactions in a perfusion bioreactor. *Frontiers in Bioengineering and Biotechnology*, 7, 221, (2019).
21. Vafai K, editor. *Handbook of porous media*. (Crc Press, 2015).
22. Arjmandi H, Zoofaghari M, Rezaei M, Kanebratt K, Vilen L, Janzen D, Gennemark P, Noel A. Diffusive Molecular Communication with a Spheroidal Receiver for Organ-on-Chip Systems. *IEEE International Conference on Communication*, Italy, Rome, May 2023.
23. Bauer S, Wennberg Huldt C, Kanebratt KP, Durieux I, Gunne D, Andersson S, Ewart L, Haynes WG, Maschmeyer I, Winter A, Ämmälä C. Functional coupling of human pancreatic islets and liver spheroids on-a-chip: Towards a novel human ex vivo type 2 diabetes model. *Scientific reports*, 7(1), 14620, (2017).
24. Rasband, W.S., ImageJ, U. S. National Institutes of Health, Bethesda, Maryland, USA, https://imagej.nih.gov/ij/, 1997-2018.

Acknowledgements (not compulsory)

This work was supported by the Engineering and Physical Sciences Research Council [EP/V030493/1].

Author contributions statement

H.A. derived the theory, implemented the simulator, co-conceived the experiment, analyzed the results, wrote the manuscript excluding Experimental Methods. K. K. conducted experiment and wrote the Experimental Methods. All authors co-conceived the idea of the manuscript and the experiment, discussed the theoretical and experimental results, and reviewed the manuscript.

Additional information

Hamidreza Arjmandi and Adam Noel declare no potential conflict of interest. Kajsa Kanebratt, Liisa Vilén, and Peter Gennemark are employed by AstraZeneca.